East European Journal of Physics. 3. 26-40 (2025)
DOI:10.26565/2312-4334-2025-3-03 ISSN 2312-4334

CONSTRAINING THE HYBRID MODEL FOR INVESTIGATING HOLOGRAPHIC DARK ENERGY IN MODIFIED GRAVITY

A.Y. Shaikh[a†], A.P. Jenekar[b]*
[a]*Department of Mathematics, Indira Gandhi Kala Mahavidyalaya, Ralegaon-445402 (M.S.), India*
[b]*Department of Mathematics, Arts, Commerce and Science College, Maregaon-445303 (M.S.), India*
**Corresponding Author E-mail: apjenekar@gmail.com*; [†]*E-mail: shaikh_2324ay@yahoo.com*
Received June 9, 2025; revised July 25, accepted August 12, 2025

This study examines the dynamism of holographic dark energy (HDE) in the background of *f*(*R*) gravity through a hypersurface-homogeneous space-time setting. Looking at how HDE affects the advancement of the Universe, we used a simplified hybrid expansion law (HEL) to derive a precise solution to the associated field equations. The study begins with the analysis of certain kinematical and physical characteristics related to the model. We applied constraints to the outlined hybrid model using observational Hubble data (OHD), which consists of 32-point data sets, in order to evaluate the model's physical certainty and feasibility. In connection with the values of parameter K that show up in our metric, three dynamically potential cosmological scenarios are outlined. Additionally, we examined various energy conditions (ECs) and discerned distinctive cosmic phases through the inspection of statefinder diagnostics and jerk parameter. The squared speed of sound parameter (v_s^2) is used to ensure the model's stability. The study corroborates the Universe's cosmic acceleration, as our findings conform to prevailing observational data, offering viable projections for future research in substantiating HDE.
Keywords: *Holographic dark energy; f(R) gravity; Homogeneous-Hypersurface space-time; Hybrid expansion law*
PACS: 04.50.Kd, 98.80.-k, 95.36.+x

1. INTRODUCTION

Contemporary cosmological observational data reflect the accelerating expansion of the cosmos explicated using type Ia supernovae by Riess [1,2] and Perlmutter [3], cosmic microwave background radiation (CMBR) by Komatsu et al. [4], weak lensing (WL), large-scale structure (LSS), and baryon acoustic oscillations (BAO) investigated by Tegmark [5] and Seljak [6]. The dark energy (DE) might explain the justification for the Universe's accelerating expansion, as it counteracts matter's natural attraction and speeds up the Universe's expansion, as outlined in [7]. Furthermore, it is estimated that this bewildering substance makes up 68.3% of the Universe, with an additional 26.8% being dark matter (DM). The equation of state (EoS), $p_{de} = \omega_{de}\rho_{de}$, with ω_{de} representing the cosmic time function known as the EoS parameter, determines DE having negative pressure along with a positive energy density [8]. Addressing the DE problem involves considering various candidates, namely, the cosmological constant [9], the X-matter [10,11] and quintessence [12,13]. The cosmological constant (Λ) has been proposed by cosmologists as a prominent candidate appropriate to DE gleaned from the several observational findings [14]. However, it encounters setbacks associated with cosmic coincidence along with fine-tuning challenges. The DE issue associated with theoretical physics remains challenging to resolve, irrespective of the substantial evidence available. A precise appraisal of the Universe's expansion rate proves vital for gaining details on the progression of this rate over eternity. The holographic dark energy (HDE) has emerged as a preferable candidate for explaining DE, which is appropriate to the holographic principle initially outlined by Hooft [15] from the perspective of black hole physics. In conformity with Susskind [16] and Bousso [17], the holographic principle proclaims that the system's entropy is contingent upon its surface area away from its volume. In further detail, Fischer and Susskind [18], in conjunction with Cohen et al. [19], presented a pioneering cosmological integration based on the holographic principle, thereby broadening its relevance far beyond the boundaries of black hole physics. Inquiry procedures in [20] reveal a holographic approach for connecting the early Universe with the Universe's late-time acceleration era, whilst extensive research in [21–24] effectively clarifies the substantial link among these HDE models and recent observational evidence.

Einstein's General Relativity (GR) is an insightful theory for interpreting gravitational circumstances; however, it fails to adequately describe DE and DM, prompting researchers to focus on its modification, which leads to various alternative theories. Modified Gravity (MG) is one such approach, focusing on deviating the space-time geometry within Einstein's equations. Several kinds of MG theories, starting with $f(R)$ gravity, $f(T)$ gravity, $f(G)$ gravity, and $f(Q)$ gravity, are being put forward in this setting. Researchers are increasingly exploring MG as a means to elucidate the Universe's cosmic acceleration and essence of DE. Buchdahl [25] commenced $f(R)$ gravity seeking to clarify the Universe's rapid expansion in addition to the progression of its formations. Starobinsky [26] presented isotropic cosmological models within $f(R)$ gravity that lacked singularities. Capozziello et al. [27] explored exact solutions for

Cite as: A.Y. Shaikh, A.P. Jenekar, East Eur. J. Phys. 3, 26 (2025), https://doi.org/10.26565/2312-4334-2025-3-03

cosmological models, while Nojiri and Odintsov [28] proposed a unified model aiming to reconcile early-time expansion combined with late-time acceleration in $f(R)$ gravity. Katore and Gore [29] delved into Bianchi type-I models, examining the interplay of HDE in the view of $f(R)$ gravity. For an in-depth probe across multiple intriguing $f(R)$ models, see ref. [30–32]. For cosmologically valuable models, $f(R)$ gravity is considered immensely appropriate out of the several MG theories. Its action is expressed as

$$S = \int \sqrt{-g}\left(f(R) + L_m\right) d^4x, \tag{1}$$

wherein $f(R)$ is the generalized function involving the Ricci scalar R, while L_m is the usual matter Lagrangian.

Variating the action appertaining to metric $g_{\mu\nu}$ comprises the relevant field equations

$$F(R)R_{\mu\nu} - \frac{1}{2}f(R)g_{\mu\nu} - \nabla_\mu\nabla_\nu F(R) + g_{\mu\nu}\nabla^\rho\nabla_\rho F(R) = -(T_{\mu\nu} + \overline{T}_{\mu\nu}), \tag{2}$$

Here $F(R) \equiv \frac{df(R)}{dR}$, ∇_μ represents covariant differentiation, $T_{\mu\nu}$ reflects the standard matter energy-momentum tensor deriving out of Lagrangian L_m whereas $\overline{T}_{\mu\nu}$ signifies the energy-momentum tensor associated with HDE.

The present work focuses on the inspection of hypersurface-homogeneous space-time concerning HDE in the setting of $f(R)$ gravity, taking into view a hybrid expansion law (HEL). We organize this article as follows. Sec. 2 addresses cosmology within the walls of hypersurface-homogeneous space–time, integrating pressureless dark matter along with the HDE framework. Sec. 3 describes the derivation of the quadrature solutions aimed at hybrid expansion in consideration of the field equations. Sec. 4 focuses on physical and kinematical properties of our model, while sec. 5 addresses the observational constraints based on Hubble data and sec. 6 explores the cosmic diagnostics. Sec. 7 comprises the ECs, whereas sec. 8 contains the statefinder diagnostics, jerk parameter, and stability analysis of the discussed model. Finally, sec. 9 presents the discussion and conclusions.

2. COSMOLOGY WITH HYPERSURFACE-HOMOGENEOUS SPACE–TIME

Some cosmological models exhibit a simple transitive homogeneity group in three dimensions, making them anisotropic, homogeneous, and particularly relevant for the purpose of explaining the isotropization and the early evolution of the cosmos, known as Bianchi type models. These models, characterized by their simplicity and effectiveness, are commonly employed in explaining the cosmic evolution. Specifically, owing to their homogeneity and anisotropy, these models are exploited to elucidate the Universe's evolution during the past phase along with its isotropic transformation. Some models fall under the category of multiply transitive, such as Kantowski–Sachs models, which lack a simple transitive subgroup. Moreover, to fully address the interaction of HDE integrated with MG, it is essential to transcend the premise of perfect isotropy. The term hypersurface model is used for a model exhibiting both multiple transitive groups as well as simple ones, combining characteristics of cosmological models that are static, spherically symmetric as well as spatially homogenous. For this reason, several authors have shown considerable interest in the inspection of hypersurface-homogeneous models, which is expressed as

$$ds^2 = -dt^2 + A^2(t)dx^2 + B^2(t)\left[dy^2 + \Sigma^2(y,K)dz^2\right], \tag{3}$$

where A and B serve as the scale factors that are functions solely of t, and $\Sigma(y,K) = \sin y, y, \sinh y$ for $K = 1, 0, -1$, respectively.

Stewart and Ellis [33] have determined considerable assistance to Einstein's field equations within the scenario when these hypersurface-homogeneous cosmological models have a perfect fluid distribution that satisfies a barotropic equation of state, whereas Singh and Beesham [34] have examined it in the existence of an adaptive anisotropic EoS parameter. Katore et al. [35] looked into hypersurface-homogeneous space-time that includes the anisotropic DE model within the boundaries of the Brans-Dicke gravity, whereas Verma et al. [36] and Katore and Shaikh [37], have observed this space-time in the setting of the Saez-Ballester gravity. Shekh and Ghaderi [38] examined this space-time, integrating an interfering HDE model by applying Hubble's and then Granda-Oliveros [39] infrared (IR) cut-off, whereas Vinutha et al. [40] observed it with the Renyi HDE by taking the Hubble horizon as a possible IR cut-off.

The scalar curvature derived from metric (3) results in

$$R = 2\left[\frac{\ddot{A}}{A} + 2\frac{\dot{A}\dot{B}}{AB} + 2\frac{\ddot{B}}{B} + \frac{\dot{B}^2}{B^2} + \frac{K}{B^2}\right], \tag{4}$$

where ‘ · ’ signifies differentiation with respect to cosmic time t.

The energy momentum tensors for HDE and pressureless matter are expressed as

$$T_{\mu\nu} = \rho_m u_\mu u_\nu ; \overline{T}_{\mu\nu} = (\rho_{de} + p_{de}) u_\mu u_\nu + g_{\mu\nu} p_{de}, \tag{5}$$

where ρ_m is the energy density of matter, p_{de} and ρ_{de} are pressure and energy density of the HDE respectively, u_μ are component of the four-velocity vector of fluid adhering to $g_{\mu\nu} u^\mu u^\nu = -1$.

Using definition of EoS parameter (ω_{de}), the energy momentum tensors (5) is articulated in the form

$$T_{\mu\nu} = \mathrm{diag}[0,0,0,-1]\rho_m ; \overline{T}_{\mu\nu} = \mathrm{diag}[\omega_{de}, \omega_{de}, \omega_{de}, -1]\rho_{de}. \tag{6}$$

Furthermore, parametric modelling turns it to

$$T_{\mu\nu} = \mathrm{diag}[0,0,0,-1]\rho_m ; \overline{T}_{\mu\nu} = \mathrm{diag}[\omega_{de} + \gamma, \omega_{de}, \omega_{de}, -1]\rho_{de}, \tag{7}$$

with the skewness parameter γ representing the variation from the EoS parameter (ω_{de}) on x-axis.

Using equations (2) and (7), the associated field equations are described as

$$F\left[\frac{\ddot{A}}{A} + 2\frac{\ddot{B}}{B}\right] - \frac{1}{2} f(R) - \left(\frac{\dot{A}}{A} + 2\frac{\dot{B}}{B}\right)\dot{F} = \rho_m + \rho_{de}, \tag{8}$$

$$F\left[\frac{\ddot{A}}{A} + 2\frac{\dot{A}\dot{B}}{AB}\right] - \frac{1}{2} f(R) - 2\frac{\dot{B}}{B}\dot{F} - \ddot{F} = -(\omega_{de} + \gamma)\rho_{de}, \tag{9}$$

and

$$F\left[\frac{\ddot{B}}{B} + \frac{\dot{A}\dot{B}}{AB} + \frac{\dot{B}^2}{B^2} + \frac{K}{B^2}\right] - \frac{1}{2} f(R) - \left(\frac{\dot{A}}{A} + \frac{\dot{B}}{B}\right)\dot{F} - \ddot{F} = -\omega_{de}\rho_{de}. \tag{10}$$

The HDE density is taken into consideration in the form

$$\rho_{de} = 3\left(\alpha H^2 + \beta \dot{H}\right), \tag{11}$$

with H representing the Hubble parameter whereas α and β are constants.

Granda and Oliveros [39] presented this condition, which must meet the constraints given by the recent observational data. The aberration in isotropic expansion is measured by the anisotropy parameter (Δ), and it plays a critical role in determining whether or not the models are appropriate for addressing isotropy. Once the directional and mean Hubble parameters of the expansion have been established, we can be parameterized the anisotropy of the expansion. The directional Hubble parameters, determining expansion rates along x, y and z axes, are respectively defined as

$$H_x = \frac{\dot{A}}{A}, \; H_y = \frac{\dot{B}}{B} = H_z. \tag{12}$$

The mean Hubble parameter is specified by

$$H = \frac{1}{3}\frac{\dot{V}}{V} = \frac{1}{3}\left(\frac{\dot{A}}{A} + 2\frac{\dot{B}}{B}\right), \tag{13}$$

with $V = AB^2$ describing the Universe's volume.

Using equations (12) and (13), the anisotropy parameter develops into

$$\Delta = \frac{2}{9H^2}\left(\frac{\dot{A}}{A} - \frac{\dot{B}}{B}\right)^2. \tag{14}$$

Using equations (9) and (10), we obtain

$$\frac{\dot{A}}{A} - \frac{\dot{B}}{B} = \frac{\lambda}{FV} + \frac{1}{FV}\int\left(\frac{KF}{B^2} - \gamma\rho_{de}\right)V dt, \tag{15}$$

where λ is a real integration constant.

Using equation (15), the anisotropy parameter (14) reduces to

$$\Delta = \frac{2}{9H^2}\left[\frac{\lambda}{FV} + \frac{1}{FV}\int\left(\frac{KF}{B^2} - \gamma p_{de}\right)Vdt\right]^2. \tag{16}$$

By opting for $\gamma = 0$ in the above equation, it can be reduced to the model that characterized by a perfect fluid distribution, making it isotropic i.e.

$$\Delta = \frac{2}{9H^2}\left[\frac{\lambda}{FV} + \frac{K}{FV}\int\frac{FV}{B^2}dt\right]^2. \tag{17}$$

The integral term in equation (16) disappears when

$$\gamma = \frac{KF}{B^2\rho_{de}}. \tag{18}$$

Consequently, the energy-momentum tensor (7) becomes

$$\overline{T}_{\mu\nu} = \mathrm{diag}\left[\omega_{de} + \frac{KF}{B^2\rho_{de}}, \omega_{de}, \omega_{de}, -1\right]\rho_{de}. \tag{19}$$

The anisotropy parameter (16) further simplifies to

$$\Delta = \frac{2\lambda^2}{9H^2F^2}V^{-2}. \tag{20}$$

We observed that the anisotropy parameter's value provided by the equation (20) resembles those obtained by several researchers pertaining to various cosmological models involving Bianchi-I [41,42], Bianchi-III [43], Bianchi-V [44,45], Bianchi-VI$_0$ [46], and hypersurface-homogenous frameworks [34-37].

3. SOLUTION TO FIELD EQUATIONS VIA HYBRID EXPANSION

Using equations (15) and (18), we obtain

$$\frac{A}{B} = c_1\exp\left(\lambda\int\frac{dt}{FV}\right), \tag{21}$$

where c_1 is integration constant.

Solving equation (21), the quadrature solutions for scale factors A and B found to be

$$A = d_1 a\exp\left[q_1\int\frac{dt}{Fa^3}\right] \text{ and } B = d_2 a\exp\left[q_2\int\frac{dt}{Fa^3}\right]. \tag{22}$$

Here $a = \left(AB^2\right)^{\frac{1}{3}} = V^{\frac{1}{3}}$ is average scale factor and $d_1 = c_1^{\frac{2}{3}}$, $d_2 = c_1^{-\frac{1}{3}}$, $q_1 = \frac{2\lambda}{3}$, $q_2 = -\frac{\lambda}{3}$, satisfying the expressions $d_1 d_2^2 = 1$ along with $q_1 + 2q_2 = 0$.

To solve the integrals in equation (22), we employ the power law relation connecting F with the average scale factor $a(t)$ as discussed by Johri and Desikan [47] in Brans-Dicke gravity. Moreover, this relation in $f(R)$ gravity is found to be $F \propto a^i$, with i being an arbitrary integer according to Kotub Uddin et al. [48] and the relation used by Sharif and Shamir [49,50], allowing us to consider $i = -2$, i.e. $F = c_2 a^{-2}$, with c_2 as a constant.

With this, the equation (22) simplifies to

$$A = d_1 a\exp\left[q_1\int\frac{dt}{a}\right] \text{ and } B = d_2 a\exp\left[q_2\int\frac{dt}{a}\right]. \tag{23}$$

We now possess a collection making up three independent equations that involve seven unknowns $A, B, \rho_m, \rho_{de}, \omega_{de}, \gamma$ and $f(R)$. To comprehensively address the system, it is necessary to incorporate further conditions, which can be established through suppositions associated with particular physical contexts or arbitrary mathematical presumptions. However, these methods are not without their constraints. Although mathematical preconceptions can create scenarios with no practical implications, physical events can sometimes emerge from complex differential

equations that are challenging to integrate. Accordingly, drawing inspiration from the work of Akarsu et al. [51], we consider a simplified HEL described by

$$V = c_3 e^{3nt} t^{3m}, \tag{24}$$

where c_3, n and m are positive constants.

From HEL model (24), it is clear that, we get exponential expansion for $m = 0$ whereas power law expansion for $n = 0$. This model exhibit accelerated volumetric expansion for $n > 1$ and $m > 1$. Consequently, the average scale factor is expressed as

$$a = k_1 e^{nt} t^m, \tag{25}$$

where $k_1 = c_3^{1/3}$.

With eqs. (23) and (25), the metric potentials are determined to be

$$A = d_1 k_1 e^{nt} t^m \exp\left(\frac{q_1}{c_2 k_1}\int \frac{dt}{e^{nt} t^m}\right) \text{ and } B = d_2 k_1 e^{nt} t^m \exp\left(\frac{q_2}{c_2 k_1}\int \frac{dt}{e^{nt} t^m}\right). \tag{26}$$

Then the metric (3) becomes

$$ds^2 = -dt^2 + d_1^2 k_1^2 e^{2nt} t^{2m} \exp\left(\frac{2q_1}{c_2 k_1}\int \frac{dt}{e^{nt} t^m}\right) dx^2 + d_2^2 k_1^2 e^{2nt} t^{2m} \exp\left(\frac{2q_2}{c_2 k_1}\int \frac{dt}{e^{nt} t^m}\right)\left[dy^2 + \Sigma^2(y, K)\, dz^2\right]. \tag{27}$$

From equation (26), it is noted that the metric potentials vanishes at starting epoch i.e. at $t = 0$ whereas becomes infinite as $t \to \infty$ indicating a big-bang type of initial singularity for the derived model.

4. PHYSICAL AND KINEMATICAL PROPERTIES

Using equations (12), (13) and (26), we obtained the directional Hubble parameters as

$$H_x = n + \frac{m}{t} + \frac{q_1}{c_2 k_1} e^{-nt} t^{-m};\ H_y = n + \frac{m}{t} + \frac{q_2}{c_2 k_1} e^{-nt} t^{-m} = H_z. \tag{28}$$

The mean Hubble parameter is determined to be

$$H = n + \frac{m}{t}. \tag{29}$$

The deceleration parameter is described by

$$q = -1 - \frac{\dot{H}}{H^2} = -1 + \frac{m}{(m + nt)^2}. \tag{30}$$

The scalar expansion θ and the shear scalar σ^2 are expressed as

$$\theta = 3H = 3\left(n + \frac{m}{t}\right), \tag{31}$$

and

$$\sigma^2 = \frac{1}{2}\left[\left(\frac{\dot{A}}{A}\right)^2 + 2\left(\frac{\dot{B}}{B}\right)^2 - \frac{1}{3}\theta^2\right] = \left(\frac{q_1^2 + 2q_2^2}{2c_2^2 k_1^2}\right) e^{-2nt} t^{-2m}. \tag{32}$$

For sufficiently large time, the expansion scalar θ shows the constant nature indicating the uniform expansion, whereas the shear scalar σ^2 vanishes; hence, there is no change in the shape of the cosmos during the evolution. Moreover, we observed that $\frac{\sigma^2}{\theta^2} \to 0$ as $t \to \infty$ indicating the Universe's isotropic expansion in later eras, it is consistent with the analysis done by Sharif and Kausar [52].

The mean anisotropic parameter (20) turns out to be

$$\Delta = \frac{2e^{-2nt} t^{2-2m} \lambda^2}{9c_2^2 k_1^2 (m + nt)^2}. \tag{33}$$

Using equations (11) and (29), the HDE parameter is found to be

$$\rho_{de}=\frac{3}{t^2}\left[\left(m+nt\right)^2\alpha-m\beta\right]. \tag{34}$$

Subsequently, the skewness parameter (18) turns out to be

$$\gamma=\frac{Kc_2\,e^{-4nt}t^{2(1-2m)}}{3d_2^2k_1^4\left(\left(m+nt\right)^2\alpha-m\beta\right)}\exp\left(-\frac{2q_2}{c_2k_1}\int\frac{dt}{e^{nt}t^m}\right). \tag{35}$$

From equation (4), the Ricci scalar is obtained as

$$R=\frac{2Ke^{-2nt}t^{-2m}}{c_2^2k_1^2d_2^2}\left(Kc_2^2\exp\left(-\frac{2q_2}{c_2k_1}\int\frac{dt}{e^{nt}t^m}\right)+3q_2^2d_2^2\right)+\frac{6}{t^2}\left(2m^2+m\left(4nt-1\right)+2n^2t^2\right). \tag{36}$$

The scalar function $f(R)$ is obtained via the Starobinsky model [53] expressed as $f(R)=R+bR^l$, with $l=2$. This model can be considered as a simple inflationary model, where *b* is an arbitrary constant representing the energy scale as discussed in [54]. A crucial aspect of considering this Starobinsky model is the existence of curvature-squared components that result in an effective cosmological constant that drives the inflationary era, resolving cosmological problems with observational evidence [55,56].

From equation (10), the matter energy density emerges as

$$\begin{aligned}\rho_m=&\frac{3q_2^2e^{-2nt}t^{-2(m+1)}}{c_2^2k_1^2}\left\{t^2+24bm^2-4bt\left(Ke^{-\frac{2q_2}{c_2k_1}\int\frac{dt}{e^{nt}t^m}}-6n^2\right)^2+12bm\left(4nt-1\right)\right\}-18bt^4q_2^4\frac{e^{-4nt}t^{-4(1+m)}}{c_2^4k_1^4}\\&-\frac{Ke^{-2nt}t^{-2(m+1)}}{d_2^2k_1^2}\left(t^2+12b\left(m(2m-1)+4mnt+2n^2t^2\right)\right)e^{-\frac{2q_2}{c_2k_1}\int\frac{dt}{e^{nt}t^m}}-2bK^2t^4\frac{e^{-4nt}t^{-4(1+m)}}{d_2^4k_1^4}e^{-\frac{4q_2}{c_2k_1}\int\frac{dt}{e^{nt}t^m}}\\&+3c_2k_1^{-2}e^{-2nt}t^{-2(m+1)}\left(3m^2-m\left(1+6nt\right)+3n^2t^2\right)-18bt^{-4}m^2\left(2m+2nt(ntm^{-2}+2)-1\right)^2\\&+\frac{e^{-4nt}t^{(4m+1)}}{c_2^2k_1^4}\left(c_2^3+q_1^2+2q_2^2\right)-3t^{-2}\left(\alpha+2\right)\left(m^2-m\left(1+\beta-2nt\right)+n^2t^2\right).\end{aligned} \tag{37}$$

Using equation (9), the expression for EoS parameter is

$$\omega_{de}=\frac{1}{3\left[\left(m+nt\right)^2\alpha-m\beta\right]}\times\left\{\begin{aligned}&\frac{e^{-2nt}t^{-2m}}{d_2^2k_1^2}\left[t^2+12b\left(m\left(2m-1\right)+4mnt+2n^2t^2\right)\right]\left(Ke^{-\frac{2q_2}{c_2k_1}\int\frac{dt}{e^{nt}t^m}}+3q_2^2d_2^2c_2^{-2}\right)\\&+3c_2^{-4}t^{-2}\left[m\left(2m-1\right)+4mnt+2n^2t^2\right]\left[t^2+6b\left(m\left(2m-1\right)+4mnt+2n^2t^2\right)\right]\\&+K\frac{e^{-4nt}t^{-2(2m-1)}}{c_2^2d_2^2k_1^4}\left[\left(12bq_2^2-c_2^3\right)e^{-\frac{2q_2}{c_2k_1}\int\frac{dt}{e^{nt}t^m}}+\frac{2Kb}{c_2^{-2}d_2^2}e^{-\frac{4q_2}{c_2k_1}\int\frac{dt}{e^{nt}t^m}}\right]\\&-3\frac{e^{-2nt}t^{-2m}}{c_2^{-1}k_1^2}\left(m^2-m+2mnt+n^2t^2\right)+\frac{18bq_2^4}{c_2^4k_1^4}e^{-4nt}t^{-2(2m-1)}\end{aligned}\right\}. \tag{38}$$

The expression for the pressure is obtained using $p_{de}=\omega_{de}\rho_{de}$, and it turns out to be

$$\begin{aligned}p_{de}=&-\frac{e^{-4nt}t^{-4m}}{d_2^2c_2^2k_1^4}\left[\left(12bq_2^2-c_2^3\right)Ke^{-\frac{2q_2}{c_2k_1}\int\frac{dt}{e^{nt}t^m}}+2K^2bc_2^2e^{-\frac{4q_2}{c_2k_1}\int\frac{dt}{e^{nt}t^m}}\right]-3c_2k_1^{-2}e^{-2nt}t^{-2(1+m)}\left(m^2-m+2mnt+n^2t^2\right)\\&+\frac{e^{-2nt}t^{-2(1+m)}}{d_2^2k_1^2}\left[\left(K+3q_2^2\right)\left(t^2+12b\left(2m^2-m+4mnt+2n^2t^2\right)\right)e^{-\frac{2q_2}{c_2k_1}\int\frac{dt}{e^{nt}t^m}}\right]-\frac{18bq_2^4}{d_2^4c_2^4k_1^4}e^{-4nt}t^{-4m}\\&+3t^{-4}\left(2m^2-m+4mnt+2n^2t^2\right)\left(t^2+6b\left(2m^2-m+4mnt+2n^2t^2\right)\right).\end{aligned} \tag{39}$$

Using the matter energy density parameter $\Omega_m = \frac{\rho_m}{3H^2}$ along with HDE density parameter $\Omega_{de} = \frac{\rho_{de}}{3H^2}$, the overall density parameter $\Omega = \Omega_m + \Omega_{de}$ is found to be

$$\Omega = \frac{1}{3(m+nt)^2} \times \left\{ \begin{array}{l} -\frac{3q_2^2 e^{-2nt} t^{-2m}}{c_2^2 k_1^2} \left[t^2 + 12b\left(m(2m-1) + 4mnt + 2n^2t^2\right) + \left(m - 3m^2 - 6mnt - 3n^2t^2\right)c_2^3 \right] \\ -Ke^{-\frac{2q_2}{c_2 k_1}\int \frac{dt}{e^{nt}t^m}} \left[\frac{e^{-2nt}t^{-2m}}{d_2^2 k_1^2}\left(t^2 + 12b\left(m(2m-1) + 4mnt + 2n^2t^2\right)\right) + \frac{12bq_2^2}{c_2^2 d_2^2 k_1^4} e^{-4nt} t^{-2m} \right] \\ +\frac{e^{-4nt}t^{-2(2m-1)}}{c_2^4 k_1^4}\left[c_2^3\left(q_1^2 + 2q_2^2\right) - 18bq_2^4 \right] - 2bK^2 \frac{e^{-4nt}t^{-2(2m-1)}}{d_2^4 k_1^4} e^{-\frac{4q_2}{c_2 k_1}\int \frac{dt}{e^{nt}t^m}} \\ -3t^{-2}\left[m(2m-1) + 4mnt + 2n^2t^2 \right]\left[t^2 + 6b\left(m(2m-1) + 4mnt + 2n^2t^2\right) \right] \end{array} \right\}. \quad (40)$$

Now, to visualize various components of our model in relation to redshift z, we employ the established relation $a(t) = \frac{a_0}{1+z}$ with $a_0 = 1$ to derive the expression for cosmic time concerning redshift as follows

$$t(z) = \left(\frac{m}{n}\right) \mathrm{W}\left(\frac{n}{m}\left[k_1(1+z)\right]^{-\frac{1}{m}} \right), \quad (41)$$

where $\mathrm{W}(x)$ is the Lambert W function [57].

Consequently, the Hubble parameter (29) in relation to redshift (z) is articulated in the form

$$H(z) = n\left\{ 1 + \left[\mathrm{W}\left(\frac{n}{m}\left[k_1(1+z)\right]^{-\frac{1}{m}} \right) \right]^{-1} \right\}. \quad (42)$$

5. OBSERVATIONAL CONSTRAINTS

We use Hubble datasets to apply constraints to our model's parameters, improving predictions and refining estimates for a more robust understanding of cosmological parameters. The Hubble constant has been computed by a number of studies [58–65] at various redshifts employing the differential age technique together with the galaxy clustering method. Table 1. lists the 32 $H(z)$ measurements, together with their associated errors $\sigma(z)$, within the redshift bounds of $0.07 \le z \le 1.965$.

Table 1. Hubble parameter $H(z)$ along with their associated errors $\sigma(z)$ over redshift (z).

z	$H(z)$ [a]	$\sigma(z_i)$	References	z	$H(z)$ [a]	$\sigma(z_i)$	References
0.07	69.0	19.6	[58]	0.4783	80.9	9.0	[61]
0.09	69.0	12.0	[59]	0.48	97.0	62.0	[63]
0.12	68.6	26.2	[58]	0.593	104.0	13.0	[60]
0.17	83.0	8.0	[59]	0.68	92.0	8.0	[60]
0.179	75.0	4.0	[60]	0.75	98.8	33.6	[64]
0.199	75.0	5.0	[60]	0.781	105.0	12.0	[60]
0.2	72.9	29.6	[58]	0.875	125.0	17.0	[60]
0.27	77.0	14.0	[59]	0.88	90.0	40.0	[63]
0.28	88.8	36.6	[58]	0.9	117.0	23.0	[59]
0.352	83.0	14.0	[60]	1.037	154.0	20.0	[60]
0.3802	83.0	13.5	[61]	1.3	168.0	17.0	[59]
0.4	95.0	17.0	[59]	1.363	160.0	33.6	[65]
0.4004	77.0	10.2	[61]	1.43	177.0	18.0	[59]
0.4247	87.1	11.2	[61]	1.53	140.0	14.0	[59]
0.4497	92.8	12.9	[61]	1.75	202.0	40.0	[59]
0.47	89.0	50.0	[62]	1.965	186.5	50.4	[65]

[a] *km s^{-1} Mpc^{-1}*

Using the eq. (42), we have determined the theoretical values of $H(z)$ in accordance with our hybrid model and applied it to constrain the model's parameters n, m and k_1. To find mean values of these parameters, the corresponding chi-square function is

$$\chi^2(n,m,k) = \sum_{i=1}^{32} \frac{\left(H_{th}(z_i;n,m,k_1) - H_{ob}(z_i)\right)^2}{\sigma^2(z_i)}, \tag{43}$$

with $H_{th}(z_i)$ and $H_{ob}(z_i)$ specify the $H(z)$'s theoretical and observed values respectively while $\sigma(z_i)$'s stands for corresponding errors in $H_{ob}(z_i)$.

Table 2. A description of best fit values derived via the minimized χ^2 -test.

Dataset	Parameters	Hybrid model
$H(z)$	n	$n = 1.45 \pm 0.34$
	m	$m = 1.15 \pm 0.01$
	k_1	$k_1 = 100 \pm 0.68$
	$\chi^2_{\min}$	$\chi^2_{\min} = 0.691$

Table 2. displays the best fit values of the model's parameters n, m and k_1 estimated via the minimized χ^2 -test. The observed Hubble data with error bars and theoretical values of Hubble parameter H according to our model is depicted in Fig. 1 which shows that the Hubble parameter H emerges as an increasing function of redshift. There is close agreement between the observed and theoretical values in the redshift range $0 < z < 1$, which validates our model in the recent past, elaborating the late matter-dominated era transitioning to DE domination, while struggling to show close agreement in the range $1 < z < 2$ in the early epoch. These deviations possibly occurred at higher redshifts $(z > 1)$, as HDE models are designed to address late-time acceleration and might not be applicable when extrapolated backwards to higher redshifts.

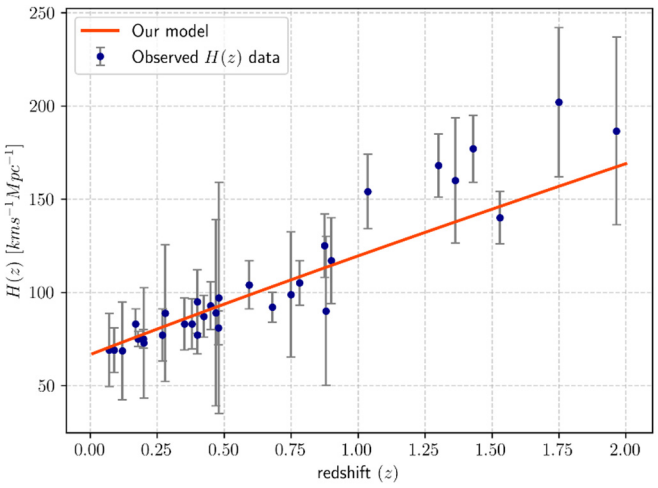

Figure 1. The inspection of Hubble Parameter H against redshift (z).

6. COSMOLOGICAL DIAGNOSTICS

The study of cosmological diagnostics is crucial for understanding how the Universe has evolved. We constructed visual illustrations of the various cosmological components, showing how they vary with redshift (z) by making use of relation (42), thereby facilitating more precise predictions and a deeper insight into cosmic dynamics. We specified a trio of situations based on $K = -1, 0, 1$ by appropriately selecting values for the various associated constants, taking reference from recent studies. We take $b = -0.1$ [66] as the negative value of b is essential for the Starobinsky model to be viable as a model of inflation, $\alpha = 10, \beta = 1$, [67] and $c_2 = 1$ while taking $n = 1.45$, $m = 1.15$ and $k_1 = 100$ based on estimated best-fit values as specified in Table 2. The variation of the skewness parameter and the anisotropic parameter against redshift is depicted in Fig. 2. The skewness parameter for $K = 1$ and anisotropic parameter both have positive values in the past, whereas in the case of $K = -1$, the skewness parameter has a negative value and is zero for $K = 0$. Consequently,

both these parameters vanish at $z \to -1$ which indicates that there is a phase transformation of the Universe in our model from anisotropy to isotropy, which leads to the attainment of the Universe's isotropization.

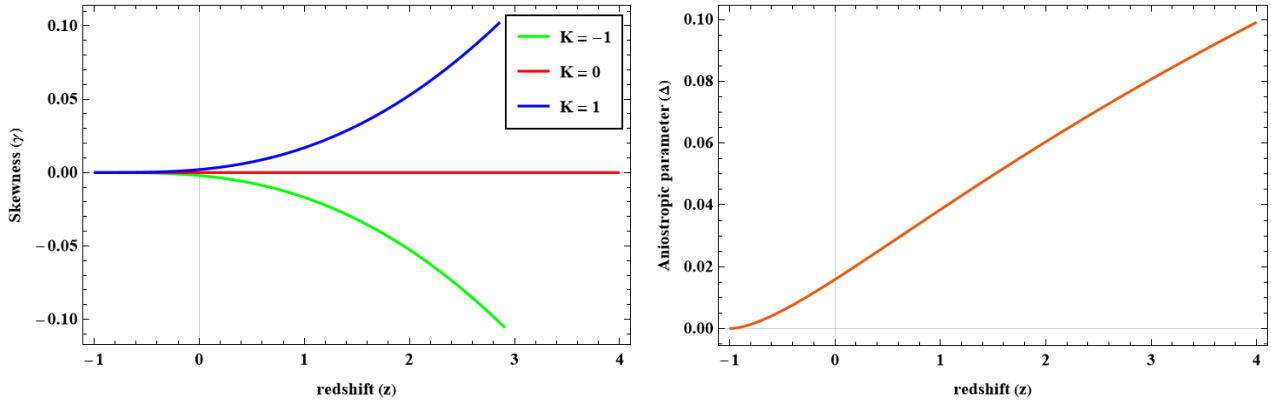

Figure 2. The variation of the skewness parameter (left panel) and the anisotropic parameter (right panel) against redshift.

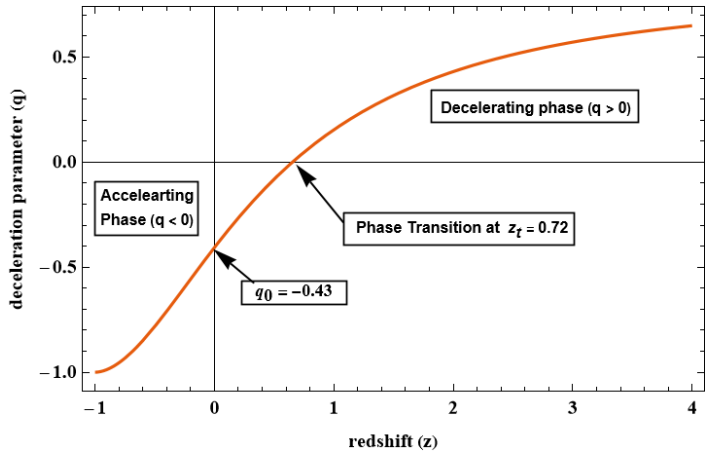

Figure 3. The approach of the deceleration parameter (q) up against redshift (z).

The sign of q serves as an indicator of detecting the accelerating or decelerating nature of the cosmos. A positive q signifies the conventional decelerating model, while a negative q indicates an accelerating Universe. Recent cosmological observations from Ade et al. [68] demonstrate that the current value of the deceleration parameter abides within the bounds of $-1 < q < 0$ as confirmed from observational data, and hence the Universe is presently undergoing acceleration, whereas it decelerated in the past. As depicted in Fig. 3, the deceleration parameter presently abides in this range, indicating the Universe's accelerated expansion, and its track reveals the progression in cosmic history, transitioning from a stage of deceleration to an instance of acceleration, with this transition happening at a point $z_t = 0.62$ that resembles with recent observational estimates of $z_{tr} = 0.60^{+0.21}_{-0.12}$ from Lu et al. [69] and $z_{tr} = 0.597^{+0.214}_{-0.214}$ from Myrzakulov et al. [70], while the present value of deceleration parameter being $q_0 = -0.43$ lies close to the widely accepted value $q_0 \approx 0.55$ as per the recent observations [71,72].

Inspecting the EoS parameter for DE is an essential component in the field of observational cosmology. The quintessence dark era occurs when $\omega_{de} > -1$, whereas phantom-dominated Universe is observed if $\omega_{de} < -1$ and the ΛCDM model for $\omega_{de} = -1$. Fig. 4 represents the cosmic progression of the EoS parameter in regard to redshift. Initially, it begins in the phantom-dominated region, and at present, it gets slightly close to -1 indicating the ΛCDM model and reaches the quintessence model in the future for all three situations. The data from SN Ia, as discussed in [73], indicates a range of $-1.67 < \omega_{de} < -0.62$, whereas considering SN Ia data combined with CMB anisotropy and galactic clumping statistics, the constrained limit becomes $-1.33 < \omega_{de} < -0.79$ as investigated by Tegmark et al. [5]. The Planck collaborations [74] provide the range $-1.26 \le \omega_{de} \le -0.92$ (Planck+WP+Union2.1) and $-1.38 \le \omega_{de} \le -0.89$ (Planck+WP+BAO). At the present epoch, the EoS parameter's value is found to be $\omega_0 = -0.931, -1.004, -1.102$ for $K = -1, 0, 1$ respectively, which thereby corresponds closely to the recent observational estimates [75].

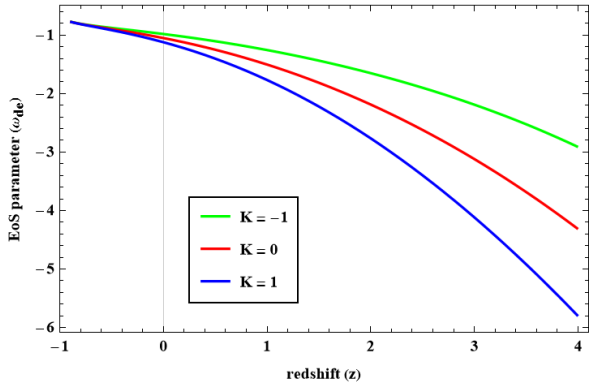

Figure 4. Progression of EoS parameter (ω_{de}) against redshift

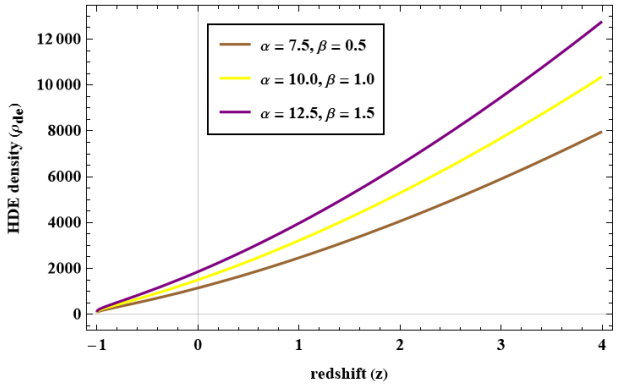

Figure 5. Plot of HDE density for various values of α and β.

The plot of HDE density with the evolution of redshift concerning different values of α and β is depicted in Fig. 5, which shows that the nature of the HDE density is positive and decreasing. It declines from a high starting value to a low ending value. Consequently, energy density drops from the past to the future, or from high to low redshift. This indicates that DE will unquestionably take control of the Universe in the future. The hypothesis that the density of matter declines whereas space grows as the Universe expands is supported by this study. As depicted in Fig. 6, the pressure stays negative throughout. This showcases more backing that the Universe expanding rapidly. The open, flat, and closed Universes are represented by the overall density parameters with $\Omega > 1$, $\Omega = 1$ and $\Omega < 1$ respectively. Fig. 7 is a graphical presentation of the overall density parameter, revealing its approach to a constant value close to 1 at late times, which suggests that the Universe tends to become flat, aligning with observational findings in accordance with the derived model [76].

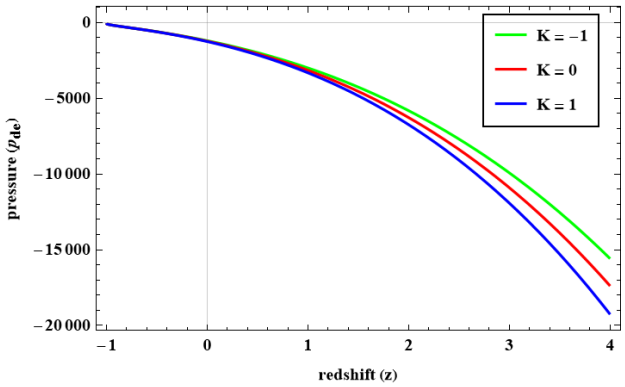

Figure 6. Plot of pressure (p_{de}) versus redshift (z).

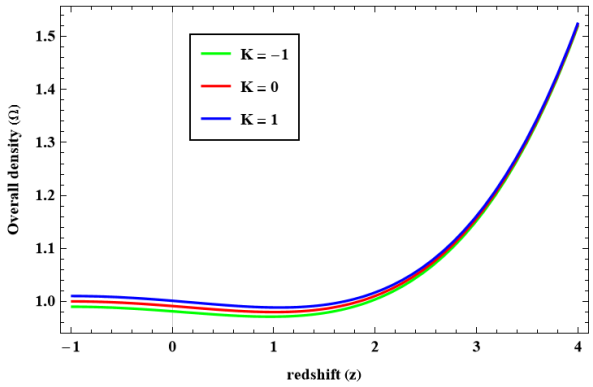

Figure 7. Plot of overall density (Ω) versus redshift (z).

7. ENERGY CONDITIONS

In $f(R)$ gravity, the Energy Conditions (ECs) have a crucial aspect in exploring the cosmological progression. It includes the null, weak, strong, and dominant ECs stated by

i. Null energy condition (NEC) $\Leftrightarrow \rho_{de} + p_{de} \geq 0$.

ii. Weak energy condition (WEC) $\Leftrightarrow \rho_{de} + p_{de} \geq 0;\ \rho_{de} \geq 0$.

iii. Strong energy condition (SEC) $\Leftrightarrow \rho_{de} + p_{de} \geq 0;\ \rho_{de} + 3p_{de} \geq 0$.

iv. Dominant energy condition (DEC) $\Leftrightarrow \rho_{de} - |p_{de}| \geq 0;\ \rho_{de} \geq 0$.

For $f(R)$ gravity, J. Santos et al. [77] obtained the NEC and SEC by applying Raychaudhuri's equation, ensuring gravity to be attractive, while the WEC and DEC were derived by comparing them with conditions derived straightway from the proficient energy-momentum tensor. Moreover, S. Capozziello et al. [78] investigate how the energy conditions can affect the cosmological evolution and the emergence of singularities in $f(R)$ gravity. The NEC asserts that as the Universe expands, its energy density will recede, and any breach of this premise could potentially lead to the Big Rip possibility for the cosmos, whereas the accelerated pace of the Universe's expansion is attributed to SEC violation.

The graphical presentations of ECs versus redshift are depicted in Fig. 8 with WEC reflected in Fig. 5. These graphical presentations of ECs specified that WEC, NEC, and DEC are considerably validated, whereas the violation of

SEC culminates in the accelerating expansion of the Universe, which is in concurrence with the current scenario of the cosmos [79,80].

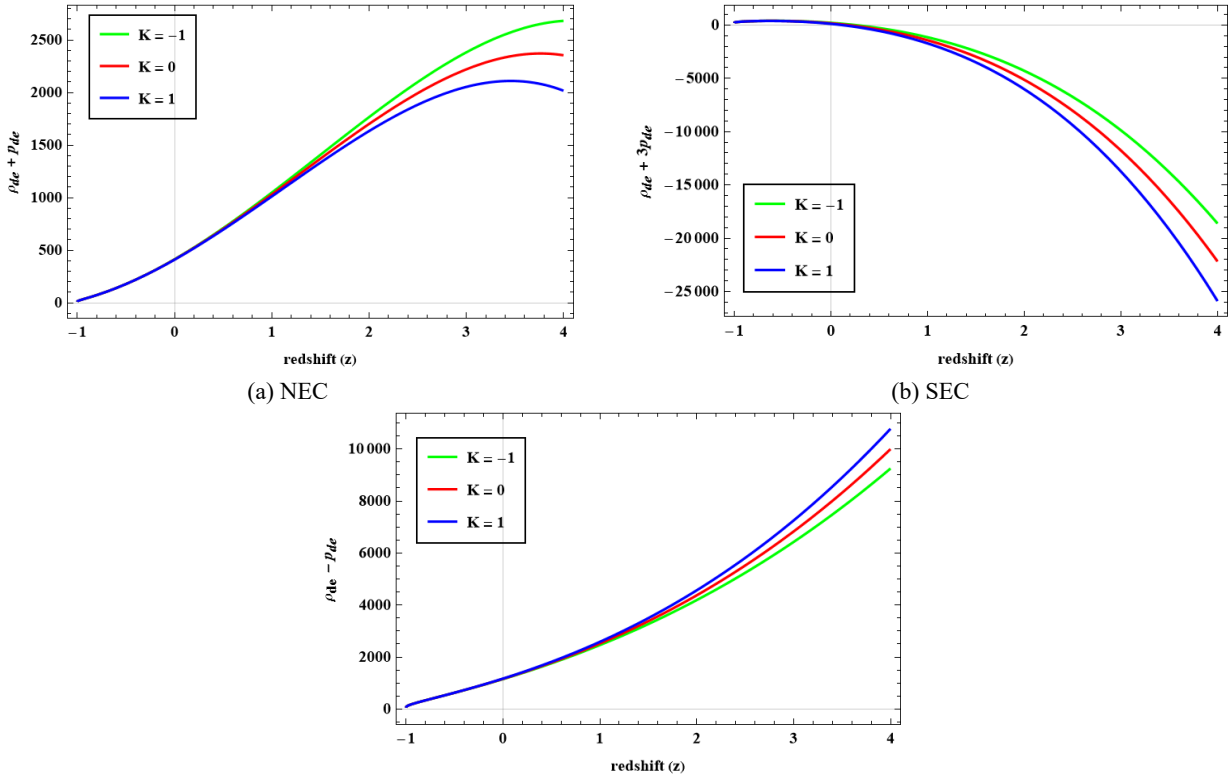

(a) NEC (b) SEC

(c) DEC

Figure 8. Profile of ECs against redshift

8. PHASE DIAGNOSTICS AND STABILITY ANALYSIS

The examination of statefinder and jerk parameters indicates variations across conventional expansion, thereby improving perception of the implications of DE models, while the stability assessment ensures our model's stability.

8.1 Statefinder Diagnostics

An investigation into the variability of the expansion of cosmos via higher-order derivatives of the expansion factor is introduced by Sahni et al. [81] as a diagnostic perspective for DE using the pairing of parameters $\{r,s\}$, with r representing jerk parameter, whereas s specifying the substance of the DE. This so-called "statefinder" is outlined below.

$$r \equiv \frac{\dddot{a}}{aH^3} \text{ and } s \equiv \frac{r-1}{3\left(q-\frac{1}{2}\right)}. \tag{44}$$

Since the statefinder is dependent on the expansion factor $\dddot{a}$ as well as the metric representing space-time, it can be considered a "geometrical" diagnostic. It effectively distinguishes between different types of cosmological models such as interacting DE models, brane models, quintessence, Chaplygin gas (CG), and cosmological constant as discussed in [82,83]. In a case of $(r,s)=(1,1)$, it signals cold dark matter (CDM), whereas $(r,s)=(1,0)$ represents the ΛCDM model. The DE regions can be specified as quintessence for $r<1$ and phantom for $s>0$, while the trajectory for the CG model belongs to the region $r>1$ with $s<0$. The statefinder settings for our HEL model are found to be $r=1-\frac{3m(m+nt)-2m}{(m+nt)^3}$ and $s=\frac{2}{3(m+nt)}-\frac{2nt}{3m^2+2m(3nt-1)+3n^2t^2}$ with their association, described by

$$\begin{aligned} r=&\frac{9ms^2(1+s)\left(m(1+s)^3-4s\right)}{4\left[2\sqrt{m^2s^9\left(9s-2m(1+s)^3\right)}+ms^3\left(6s^2-6ms(1+s)^3+m^2(1+s)^6\right)\right]^{1/3}}+\frac{9}{4}(m-2)s+\frac{9}{2}ms^2\\ &+\frac{9}{4}\left[2\sqrt{m^2s^9\left(9s-2m(1+s)^3\right)}+ms^3\left(6s^2-6ms(1+s)^3+m^2(1+s)^6\right)\right]^{1/3}+\frac{9}{4}ms^3+1. \end{aligned} \tag{45}$$

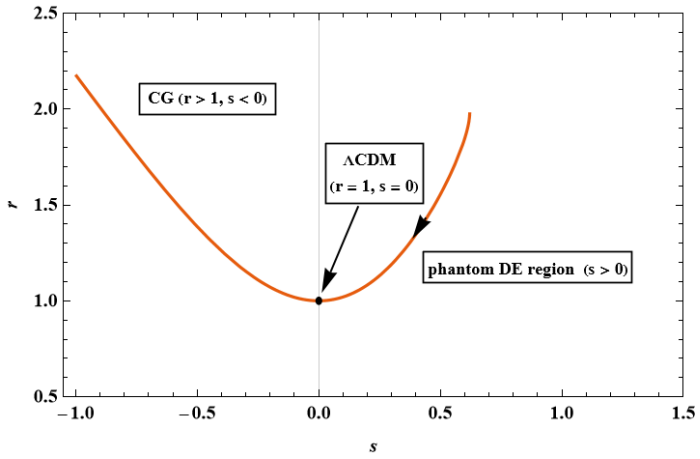

Figure 9. Plot of r vs s .

Fig. 9 illustrates the variation of r across s, suggesting that the state finder measurements will precisely correspond along the lines of the ΛCDM model in the near future. The resulting alignment progresses seamlessly toward the ΛCDM point while incorporating the CG and even Phantom DE portions.

8.2 Jerk Parameter

This parameter serves the purpose of recognizing models that conform to the ΛCDM model. A negative deceleration parameter accompanied by a positive jerk value reflects transitions between acceleration and deceleration phases. The jerk parameter of our model appears to be

$$j(t)=\frac{1}{H^3}\frac{\dddot{a}}{a}=1-\frac{m\left(3nt+3m-2\right)}{\left(m+nt\right)^3}. \tag{46}$$

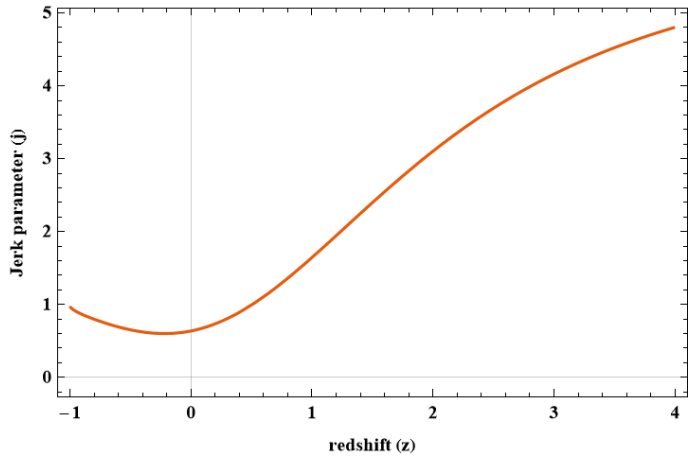

Figure 10. The plot of jerk parameter against redshift

For $j=1$, it is identified to be the ΛCDM model. Fig. 10 presents the variations of the jerk parameter against redshift, which reflects a declining trend of the jerk parameter until it attains one as $z\to -1$, thus sustaining the model's conformity with the ΛCDM model based on the observational evidence [84].

8.3 Stability Analysis

To verify the stability of our model, we utilized the squared speed of sound parameter v_s^2, defined by $v_s^2=dp_{de}/d\rho_{de}$, as proposed by Sadeghi et al. [85]. If the value of v_s^2 is positive, this implies that the model is stable, whereas it is unstable for a negative value of v_s^2. Using equations (34) and (39), the stability parameter v_s^2 for our model is obtained, and its graphical visualization over the redshift is presented in Fig. 11, which shows a positive nature for all three situations thoroughly over the course of progression, indicating our model's stability.

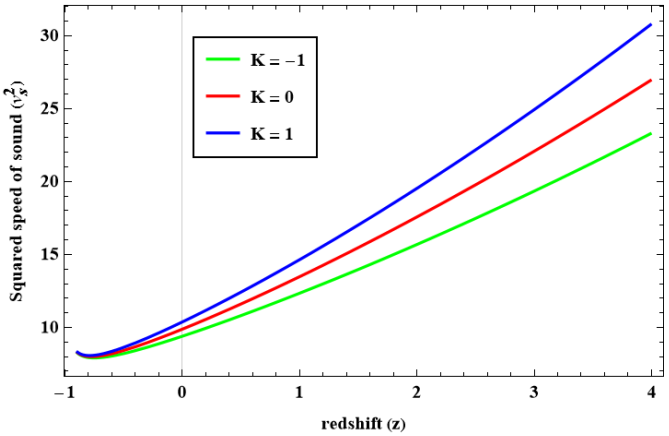

Figure 11. The variation of plot of squared speed of sound (v_s^2) against redshift.

9. CONCLUSIONS

This article is engrossed to delve into hypersurface-homogeneous metric from the perspective of $f(R)$ gravity. Having an account of two fluids viz pressureless matter together with HDE, the field equations are assimilated, and their solutions are estimated by taking simplified HEL accompanied by the Starobinsky model [53]. By using OHD with 32-point datasets, observational constraints are applied to examine the physical dependability and feasibility of the model. We observed that Hubble parameter H emerges as increasing function of redshift z as illustrated in Fig. 1 which shows that there is a close agreement between the observed and theoretical values of H in the redshift range $0<z<1$, elaborating the late matter-dominated era transitioning to dark energy domination, which eventually validates our model. From the graphical presentations of various parameters pertaining to redshift involving three cases of $K=0,1,-1$, we observed the following implications:

- Both the skewness (γ) and anisotropic parameter (Δ) tend to zero at $z\to -1$ as reflected in Fig. 2, thereby satisfying the isotropization of the Universe which is additionally supported by the fact that the ratio of expansion scalar θ and shear scalar σ^2 tends to zero at later times.
- The model effectively allows for the transition from decelerated to rapid expansion. The deceleration parameter progresses from positive to negative, transitioning from a stage of deceleration to an instance of acceleration as shown in Fig. 3, with the transition point $z_t=0.62$ resembling the observational estimates in [69,70].
- Fig. 4 outlined the cosmic progression of the EoS parameter (ω_{de}) in regard to redshift, which shows that it begins from a phantom-dominated region initially, and at present, it gets slightly close to -1 indicating the ΛCDM model, whereas it reaches to the quintessence model in the future. Moreover, the EoS parameter's current values, $\omega_0=-0.931,-1.004,-1.102$ for $K=0,1,-1$, respectively, are consistent with the values observed in recent cosmological data [75].
- The hypothesis that the density of matter declines and space grows as the Universe expands is supported by the positive and decreasing nature of HDE density (ρ_{de}) with the evolution of redshift as shown in Fig. 5. The pressure (p_{de}) stays negative over the course of the evolution of our model, as reflected in Fig. 6. This lends reassurance to the conceptualization that the cosmos is expanding at a faster pace. The approach of the overall density (Ω) parameter revealed that it tends to a constant value slightly close to 1 at late times, as displayed in Fig. 7, thereby implying that the Universe tends to become flat in the future, aligning with observational findings of [76] in accordance with the derived model.
- From the variability of ECs as reflected in Figs. 5 and 8, we found that WEC, NEC, and DEC are considerably validated, whereas the violation of SEC culminates in the accelerating expansion of the cosmos, which is in concurrence with the current scenario of the cosmos.
- It is observed from statefinder diagnostics as shown in Fig. 9 that our model tends to approach the ΛCDM model in the near future. Fig. 10 reflects a declining trend of the jerk parameter until it attains one as $z\to -1$, thus, sustaining the model's conformity with the ΛCDM model based on the observational evidence [84].
- Our model's stability is established via the squared speed of sound (v_s^2) parameter as illustrated in Fig. 11, which shows a positive nature thoroughly over the course of progression of redshift, thereby indicating the stable nature of our model.

Based on the preceding discussion, it is evident that our study's findings concur with existing observational data, which supports our interpretation of the Universe's cosmic acceleration and enables us to make specific predictions that can be tested with forthcoming cosmological probes.

Data availability statement

The study described in this paper didn't generate any new data.

Acknowledgments

The authors express their sincere gratitude to the editor and the anonymous reviewer(s) for their insightful comments and constructive suggestions, which have greatly enhanced the quality and clarity of the manuscript.

ORCID

A.Y. Shaikh, https://orcid.org/0000-0001-5315-559X; **A.P. Jenekar**, https://orcid.org/0009-0005-8928-3725

REFERENCES

[1] A.G. Riess, *et al.*, Astron. J. **116**, 1009 (1998). https://doi.org/10.1086/300499
[2] A. G. Riess, *et al.*, Astron. J. **117**, 707 (1999). https://doi.org/10.1086/300738
[3] S. Perlmutter, *et al.*, Astrophys. J. **517**, 565 (1999). https://doi.org/10.1086/307221
[4] E. Komatsu, *et al.*, Astrophys. J. Suppl. Ser. **192**, 18 (2011). https://doi.org/10.1088/0067-0049/192/2/18
[5] M. Tegmark, *et al.*, Phys. Rev. D **69**, 103501 (2004). https://doi.org/10.1103/PhysRevD.69.103501
[6] U. Seljak, *et al.*, Phys. Rev. D **71**, 103515 (2005). https://doi.org/10.1103/PhysRevD.71.103515
[7] K. Bamba, *et al.*, Astrophys. Space Sci. **342**, 155 (2012). https://doi.org/10.1007/s10509-012-1181-8
[8] M. Sharif, and M. Zubair, Astrophys. Space Sci. **330**, 399 (2010). https://doi.org/10.1007/s10509-010-0414-y
[9] S. M. Carroll, *et al.*, Annu. Rev. Astron. Astrophys. **30**, 499 (1992). https://doi.org/10.1146/annurev.aa.30.090192.002435
[10] M. S. Turner, and M. White, Phys. Rev. D **56**, R4439 (1997). https://doi.org/10.1103/PhysRevD.56.R4439
[11] Z.-H. Zhu, M.-K. Fujimoto, and D. Tatsumi, Astron. Astrophys. **372**, 377 (2001). https://doi.org/10.1051/0004-6361:20010458
[12] B. Ratra, and P. J. E. Peebles, Phys. Rev. D **37**, 3406 (1988). https://doi.org/10.1103/PhysRevD.37.3406
[13] V. Sahni, and L. Wang, Phys. Rev. D **62**, 103517 (2000). https://doi.org/10.1103/PhysRevD.62.103517
[14] S. Weinberg, Rev. Mod. Phys. **61**, 1 (1989). https://doi.org/10.1103/RevModPhys.61.1
[15] G.'t Hooft, (Conf. Proc. C, **284**, 930308 (1993). https://doi.org/10.48550/arXiv.gr-qc/9310026
[16] L. Susskind, and J. Uglum, Phys. Rev. D **50**, 2700 (1994). https://doi.org/10.1103/PhysRevD.50.2700
[17] R. Bousso, J. High Energy Phys. **1999**, 004 (1999). https://doi.org/10.1088/1126-6708/1999/07/004
[18] W. Fischler, and L. Susskind, arXiv:hep-th/9806039 (1998). https://doi.org/10.48550/arXiv.hep-th/9806039
[19] A. G. Cohen, D. B. Kaplan, and A. E. Nelson, Phys. Rev. Lett. **82**, 4971 (1999). https://doi.org/10.1103/PhysRevLett.82.4971
[20] S. Nojiri, *et al.*, Phys. Rev. D **102**, (2020). https://doi.org/10.1103/physrevd.102.023540
[21] X. Zhang, Phys. Rev. D **79**, 103509 (2009). https://doi.org/10.1103/PhysRevD.79.103509
[22] L. Xu, and Y. Wang, J. Cosmol. Astropart. Phys. **2010**, 002 (2010). https://doi.org/10.1088/1475-7516/2010/06/002
[23] Y. Wang, and L. Xu, Phys. Rev. D **81**, 083523 (2010). https://doi.org/10.1103/PhysRevD.81.083523
[24] I. Durán, and D. Pavón, Phys. Rev. D **83**, 023504 (2011). https://doi.org/10.1103/PhysRevD.83.023504
[25] H. A. Buchdahl, Mon. Not. R. Astron. Soc. **150**, 1 (1970). https://doi.org/10.1093/mnras/150.1.1
[26] A. A. Starobinsky, Phys. Lett. B **91**, 99 (1980). https://doi.org/10.1016/0370-2693(80)90670-X
[27] S. Capozziello, P. Martin-Moruno, and C. Rubano, Phys. Lett. B **664**, 12 (2008). https://doi.org/10.1016/j.physletb.2008.04.061
[28] S. Nojiri, and S. D. Odintsov, arXiv:0807.0685 [hep-th] (2008). https://doi.org/10.48550/arXiv.0807.0685
[29] S. D. Katore, and S. V. Gore, J. Astrophys. Astron. **41**, 12 (2020). https://doi.org/10.1007/s12036-020-09632-z
[30] A. De Felice, and S. Tsujikawa, Living Rev. Relativ. **13**, 3 (2010). https://doi.org/10.12942/lrr-2010-3
[31] T. P. Sotiriou, and V. Faraoni, Rev. Mod. Phys. **82**, 451 (2010). https://doi.org/10.1103/RevModPhys.82.451
[32] S. Nojiri, and S. D. Odintsov, Phys. Rep. **505**, 59 (2011). https://doi.org/10.1016/j.physrep.2011.04.001
[33] J. M. Stewart, and G. F. R. Ellis, J. Math. Phys. **9**, 1072 (1968). https://doi.org/10.1063/1.1664679
[34] C. P. Singh, and A. Beesham, Gravit. Cosmol. **17**, 284 (2011). https://doi.org/10.1134/S020228931103008X
[35] S. D. Katore, *et al.*, Commun. Theor. Phys. **62**, 768 (2014). https://doi.org/10.1088/0253-6102/62/5/21
[36] M. K. Verma, S. Chandel, and S. Ram, Pramana **88**, 8 (2017). https://doi.org/10.1007/s12043-016-1317-4
[37] S. D. Katore, and A. Y. Shaikh, Astrophys. Space Sci. **357**, 27 (2015). https://doi.org/10.1007/s10509-015-2297-4
[38] S. H. Shekh, and K. Ghaderi, Phys. Dark Universe **31**, 100785 (2021). https://doi.org/10.1016/j.dark.2021.100785
[39] L. N. Granda, and A. Oliveros, Phys. Lett. B **669**, 275 (2008). https://doi.org/10.1016/j.physletb.2008.10.017
[40] T. Vinutha, *et al.*, Int. J. Geom. Methods Mod. Phys. **20**, 2350119 (2023). https://doi.org/10.1142/S0219887823501190
[41] S. Kumar, and C. P. Singh, Astrophys. Space Sci. **312**, 57 (2007). https://doi.org/10.1007/s10509-007-9623-4
[42] Ö. Akarsu, and C. B. Kılınç, Gen. Relativ. Gravit. **42**, 119 (2009). https://doi.org/10.1007/s10714-009-0821-y
[43] Ö. Akarsu, and C. B. Kılınç, Gen. Relativ. Gravit. **42**, 763 (2010). https://doi.org/10.1007/s10714-009-0878-7
[44] C. P. Singh, *et al.*, Astrophys. Space Sci. **315**, 181 (2008). https://doi.org/10.1007/s10509-008-9811-x
[45] J. P. Singh, and P. S. Baghel, Int. J. Theor. Phys. **48**, 449 (2009). https://doi.org/10.1007/s10773-008-9820-0
[46] K. S. Adhav, *et al.*, Astrophys. Space Sci. **332**, 497 (2011). https://doi.org/10.1007/s10509-010-0519-3
[47] V. B. Johri, and K. Desikan, Gen. Relativ. Gravit. **26**, 1217 (1994). https://doi.org/10.1007/BF02106714
[48] K. Uddin, J. E. Lidsey, and R. Tavakol, Class. Quantum Gravity **24**, 3951 (2007). https://doi.org/10.1088/0264-9381/24/15/012
[49] M. Sharif, and M. F. Shamir, Class. Quantum Gravity **26**, 235020 (2009). https://doi.org/10.1088/0264-9381/26/23/235020
[50] M. Sharif, and M. F. Shamir, Mod. Phys. Lett. A **25**, 1281 (2010). https://doi.org/10.1142/S0217732310032536
[51] Ö. Akarsu, *et al.*, J. Cosmol. Astropart. Phys. **2014**, 022 (2014). https://doi.org/10.1088/1475-7516/2014/01/022
[52] M. Sharif, and H. R. Kausar, Phys. Lett. B **697**, 1 (2011). https://doi.org/10.1016/j.physletb.2011.01.027
[53] A. A. Starobinsky, JETP Lett. **86**, 157 (2007). https://doi.org/10.1134/S0021364007150027
[54] Y. Younesizadeh, and A. Rezaie, Int. J. Mod. Phys. A **37**, 2250040 (2022). https://doi.org/10.1142/S0217751X22500403
[55] A. S. Koshelev, *et al.*, J. High Energy Phys. **2018**, (2018). https://doi.org/10.1007/jhep03(2018)071
[56] G. Germán, J. C. Hidalgo, and L. E. Padilla, Eur. Phys. J. Plus **139**, (2024). https://doi.org/10.1140/epjp/s13360-024-05065-7

[57] R. M. Corless, *et al.*, Adv. Comput. Math. **5**, 329 (1996). https://doi.org/10.1007/BF02124750
[58] C. Zhang, *et al.*, Res. Astron. Astrophys. **14**, 1221 (2014). https://doi.org/10.1088/1674-4527/14/10/002
[59] J. Simon, L. Verde, and R. Jimenez, Phys. Rev. D **71**, 123001 (2005). https://doi.org/10.1103/PhysRevD.71.123001
[60] M. Moresco, *et al.*, J. Cosmol. Astropart. Phys. **2012**, 006 (2012). https://doi.org/10.1088/1475-7516/2012/08/006
[61] M. Moresco, *et al.*, J. Cosmol. Astropart. Phys. **2016**, 014 (2016). https://doi.org/10.1088/1475-7516/2016/05/014
[62] A. L. Ratsimbazafy, *et al.*, Mon. Not. R. Astron. Soc. **467**, 3239 (2017). https://doi.org/10.1093/mnras/stx301
[63] D. Stern, *et al.*, J. Cosmol. Astropart. Phys. **2010**, 008 (2010). https://doi.org/10.1088/1475-7516/2010/02/008
[64] N. Borghi, M. Moresco, and A. Cimatti, Astrophys. J. Lett. **928**, L4 (2022). https://doi.org/10.3847/2041-8213/ac3fb2
[65] M. Moresco, Mon. Not. R. Astron. Soc. Lett. **450**, L16 (2015). https://doi.org/10.1093/mnrasl/slv037
[66] P. H. R. S. Moraes, *et al.*, Adv. Astron. **2019**, 1 (2019). https://doi.org/10.1155/2019/8574798
[67] M. T. Manoharan, Eur. Phys. J. C **84**, (2024). https://doi.org/10.1140/epjc/s10052-024-12926-z
[68] P. A. R. Ade, *et al.*, Astron. Astrophys. **571**, A16 (2014). https://doi.org/10.1051/0004-6361/201321591
[69] J. Lu, L. Xu, and M. Liu, Phys. Lett. B **699**, 246 (2011). https://doi.org/10.1016/j.physletb.2011.04.022
[70] Y. Myrzakulov, *et al.*, Nucl. Phys. B **1016**, 116916 (2025). https://doi.org/10.1016/j.nuclphysb.2025.116916
[71] A. Kolhatkar, S. S. Mishra, and P. K. Sahoo, Eur. Phys. J. C **84**, (2024). https://doi.org/10.1140/epjc/s10052-024-13237-z
[72] D. M. Naik, *et al.*, Phys. Lett. B **844**, 138117 (2023). https://doi.org/10.1016/j.physletb.2023.138117
[73] R. A. Knop, *et al.*, Astrophys. J. **598**, 102 (2003). https://doi.org/10.1086/378560
[74] Planck Collaboration, *et al.*, Astron. Astrophys. **641**, A6 (2020). https://doi.org/10.1051/0004-6361/201833910
[75] M. Jaber, and A. de la Macorra, Astropart. Phys. **97**, 130 (2018). https://doi.org/10.1016/j.astropartphys.2017.11.007
[76] S. Kumar, Astrophys. Space Sci. **332**, 449 (2011). https://doi.org/10.1007/s10509-010-0540-6
[77] J. Santos, *et al.*, Phys. Rev. D **76**, 083513 (2007). https://doi.org/10.1103/PhysRevD.76.083513
[78] S. Capozziello, S. Nojiri, and S. D. Odintsov, Phys. Lett. B **781**, 99 (2018). https://doi.org/10.1016/j.physletb.2018.03.064
[79] A. Y. Shaikh, Eur. Phys. J. Plus **138**, 301 (2023). https://doi.org/10.1140/epjp/s13360-023-03931-4
[80] A. Y. Shaikh, Indian J. Phys. (2024). https://doi.org/10.1007/s12648-024-03151-1
[81] V. Sahni, *et al.*, J. Exp. Theor. Phys. Lett. **77**, 201 (2003). https://doi.org/10.1134/1.1574831
[82] U. Alam, *et al.*, Mon. Not. R. Astron. Soc. **344**, 1057 (2003). https://doi.org/10.1046/j.1365-8711.2003.06871.x
[83] W. Zimdahl, and D. Pavón, Gen. Relativ. Gravit. **36**, 1483 (2004). https://doi.org/10.1023/B:GERG.0000022584.54115.9e
[84] A. Al Mamon, and K. Bamba, Eur. Phys. J. C **78**, 862 (2018). https://doi.org/10.1140/epjc/s10052-018-6355-2
[85] J. Sadeghi, A. R. Amani, and N. Tahmasbi, Astrophys. Space Sci. **348**, 559 (2013). https://doi.org/10.1007/s10509-013-1579-y

ОБМЕЖЕННЯ ГІБРИДНОЇ МОДЕЛІ ДЛЯ ДОСЛІДЖЕННЯ ГОЛОГРАФІЧНОЇ ТЕМНОЇ ЕНЕРГІЇ В МОДИФІКОВАНІЙ ГРАВІТАЦІЇ

А.Й. Шейх[a], А.П. Дженекар[b]
[a]Кафедра математики, Індіра Ганді Кала Махавідьялая, Ралегаон-445402 (магістр наук), Індія
[b]Кафедра математики, коледжа мистецтв, комерції та науки, Марегаон-445303 (M.S.), Індія

У цьому дослідженні розглядається динамізм голографічної темної енергії (ГТЕ) на тлі гравітації через гіперповерхнево-однорідний просторово-часовий контекст. Розглядаючи, як ГТЕ впливає на розвиток Всесвіту, ми використали спрощений гібридний закон розширення (ГЗР) для отримання точного розв'язку пов'язаних з ним рівнянь поля. Дослідження починається з аналізу певних кінематичних та фізичних характеристик, пов'язаних з моделлю. Ми застосували обмеження до окресленої гібридної моделі, використовуючи дані спостережень Хаббла (OHD), які складаються з 32-точкових наборів даних, щоб оцінити фізичну достовірність та доцільність моделі. У зв'язку зі значеннями параметрів, що відображаються в нашій метриці, окреслено три динамічно потенційні космологічні сценарії. Крім того, ми дослідили різні енергетичні умови (ЕС) та виділили окремі космічні фази за допомогою перевірки діагностики statefinder та параметра ривка. Квадрат швидкості звуку v_s^2 використовується для забезпечення стабільності моделі. Дослідження підтверджує космічне прискорення Всесвіту, оскільки наші висновки відповідають переважаючим даним спостережень, пропонуючи життєздатні прогнози для майбутніх досліджень з обгрунтування HDE.

Ключові слова: *голографічна темна енергія; гравітація; однорідний гіперповерхневий простір-час; гібридний закон розширення*